# Circular Intensity Differential Scattering Reveals Internal Structure of Polymer Fibrils

*Ashish Sharma,[1] Alison Campbell,[1] Julien Leoni,[1] Yen Theng Cheng,[2] Markus Müllner,[2] Girish Lakhwani[1]**

[1]ARC Centre of Excellence in Exciton Science, School of Chemistry, The University of Sydney, NSW 2006, Australia.

[2]Key Centre for Polymers and Colloids, School of Chemistry, The University of Sydney, NSW 2006, Australia.

**Corresponding author***email: girish.lakhwani@sydney.edu.au

**Abstract.** The optical and electronic properties of π-conjugated polymers in organic electronic devices depend on their intra and inter-chain interactions, dictated by the internal arrangement of the polymer chains in an amorphous or semi-crystalline aggregated state. Here, we discuss the utility of circular intensity differential scattering (CIDS) of circularly polarized light as a sensitive probe to identify the internal arrangement of the polymer chains in helical polymer aggregates. We advance existing theoretical models to utilize the CIDS response and extract structural properties such as the size, orientation and periodicity of a polymer aggregate. As an example, we analyze the CIDS signatures of helically assembled fibrillar aggregates of a chiral polymer poly[(9,9-di-n-octylfluorenyl-2,7-diyl)-alt-(benzothiadiazole)](PFBT) in solution and reveal that PFBT fibrils incorporate at least 5 intertwined polymer chains. We anticipate our approach can be extended more generally to investigate the internal arrangement of supramolecular assemblies of wide range of fibrillar aggregates of π-conjugated polymers.

**TOC Graphic**

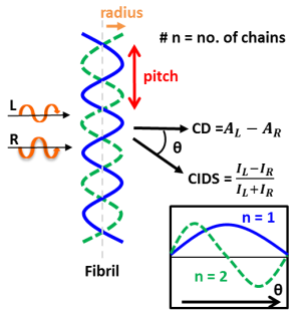

π-conjugated polymers have attracted immense interest owing to their application as active layer materials in solution-processed organic electronic devices.[1] The efficiency of these devices critically depends on the polymer morphology, which is intimately related to the aggregation state of the polymer chains.[2-3] Notably, the aggregation of polymer chains into fibrillar networks has come up as a promising strategy to improve device performance of bulk heterojunction organic solar cells (OSCs), with efficiencies reaching as high as 12.7 % for OSCs with optimized fibril morphology.[4] As polymer aggregate morphology is highly influenced by the nature of inter-chain interactions, parameters like backbone molecular structure,[5] side-chain geometry,[6] molecular weight,[7] solvent,[6, 8] and thermal history[9] influence the internal arrangement of polymer chains in the aggregate or fibril. Understanding the internal arrangement of the polymer chains into fibrillar geometries is necessary not only to identify the origin of fibril morphology, but also to determine optimum device fabrication processing conditions.

X-ray and neutron-based scattering techniques have been used in the past to identify the dimensions of polymer fibrils in solution, provided fibrils are ordered (crystalline)and the polymer concentration is significant (~1 wt%).[10-12] Detailed insights into the internal structure of the fibrils such as backbone conformation, side-chain arrangement and inter-chain stacking can also be obtained by x-ray diffraction measurements provided the assembled fibrils are well-aligned.[13-15] This limits their application in the investigation of spontaneously assembled, poorly ordered polymer fibrils, which are routinely observed during the aggregation of conjugated polymers such as in the case of polyfluorenes,[16] polythiophenes[17] and phenylvinylenes[18]. Probing the internal arrangement of polymer chains in fibrils, not limited to the specific case of ordered geometries, necessitates sensitive investigation on individually dispersed fibrils in dilute solutions (<0.1 wt%); a regime which is hitherto inaccessible by standard scattering based techniques such as wide and small angle x-ray scattering.

In the case where polymer aggregates are helical in nature, chirality can be exploited as a sensitive reporter of its internal structure (handedness, pitch, radius). Specifically, the difference in the scattered intensities of left (L) and right (R) circularly polarized light, known as circular intensity differential scattering (CIDS), can be used to extract valuable information on the geometry, periodicity and orientation of the aggregate. Seminal contributions from Bustamante[19-21], Nicolini[22], Maestre[23], Tinoco[21, 24], Hunt[25] and coworkers in both theory and experiment have demonstrated the potential of utilizing CIDS to identify the internal structure of protein aggregates , chiral nanoparticles,[26] cholesteric liquid crystals[21, 27-28] and helically-organized macro domains in biological systems[29]. The extraordinary sensitivity of the CIDS response to varied aggregate structures in dilute solutions allows it to be used as a novel spectroscopic probe of the internal arrangement of polymer chains in aggregates and fibrils. However, to best of our knowledge, there is no report demonstrating the application of CIDS to investigate the internal structure of supramolecular assemblies of π-conjugated polymers.

In this report, we advance the discussed CIDS model[19-20] for structures beyond a single polymer chain to include an orientationally averaged supramolecular bundle of intertwined helical chains. We outline a general relationship between excitation wavelength dependent CIDS spectral features and their associated helical polymer aggregate geometries that are frequently reported in literature. We demonstrate the utility of this extended model by reproducing CIDS experiments carried on a dilute solution (~0.01 wt%) of aggregates of a chiral polyfluorene copolymer, poly[(9,9-di-n-octylfluorenyl-2,7-diyl)-alt-(benzothiadiazole)] (PFBT). With the help of fluorescence detected circular dichroism (FDCD), we decouple the chiroptical response arising from differential absorbance of L and R circularly polarized light, known as circular dichroism (CD) and CIDS. AFM reveals aggregates are fibrillar in nature. Using a home-built setup, we probe CIDS as a function of fibril size. Our model is able to reproduce the experimental results and demonstrate the internal structure of PFBT fibril to comprise of at least 5 polymer chains. Furthermore, we show that these fibrils are building blocks for larger spherulites

formed in concentrated solutions. Our findings are consistent with other reports in literature[28, 30-31] that propose cholesteric phases in thin films of polyfluorenes arise from long-range hierarchical arrangement of fibrils.

CIDS is defined as

$$\mathrm{CIDS} = \frac{\mathrm{I_L}(\mathrm{r},\theta,\varphi) - \mathrm{I_R}(\mathrm{r},\theta,\varphi)}{\mathrm{I_L}(\mathrm{r},\theta,\varphi) + \mathrm{I_R}(\mathrm{r},\theta,\varphi)} \quad (1)$$

where $\mathrm{I_L}(\mathrm{r},\theta,\varphi)$ and $\mathrm{I_R}(\mathrm{r},\theta,\varphi)$ are scattered light intensities for L and R excitations, respectively, as a function of spherical coordinates given by the radial distance $(\mathrm{r})$, the azimuthal angle $(\theta)$ and the polar angle $(\varphi)$. In the case of a non-aligned periodic structure such as a rotationally averaged helix, the shape and magnitude of CIDS as a function $\theta$ can be directly related to its helical pitch and radius. A thin-wire helical polymer chain defined by the pitch ($P$) and radius ($a$) can be modeled as an array of point-polarizable scatterers whose position vectors $(R_i, R_j)$ map out a helix geometry and the polarizibility vectors ($\widehat{t_i}, \widehat{t_j}$) are defined along the tangential direction (Figure 1a). Further, we define the length of a polymer chain to be significantly larger (in the order of magnitude) than the pitch. We consider a fibril to be a bundle of N identical helical chains displaced with respect to each other along the helical axis. Figure 1a illustrates a fibril made up of 2 intertwined polymer chains. Within the first Born approximation, the differential scattering intensity $(I_L - I_R)$ can be calculated using the general analytical expression calculated by Shapiro et al.[25, 32] (equation 5). The double sum in equation 5 can then be calculated, considering all possible permutations of the inter-particle separation vector $(R_{ij})$, to arrive at the differential scattering intensity. Similarly, the expression of the total scattered intensity can be obtained, to calculate the ratio CIDS as a function of $\theta$.

$$R_i = a\cos(i\tau_0)\hat{x} + a\sin(i\tau_0)\hat{y} + \frac{Pi\tau_0}{2\pi}\hat{z} \quad (2)$$

$$R_{ij} = R_i - R_j \tag{3}$$

$$q = \frac{4\pi|R_{ij}|}{\lambda} \sin\frac{\theta}{2} \tag{4}$$

$$(I_L - I_R)(\theta) = \pi^2 \left\{ \sum_i \sum_j \left\{ \left[ \frac{8j_2}{q} \left( (\widehat{t_i} \cdot \widehat{R_{ij}})(\widehat{t_j} \cdot \widehat{R_{ij}}) \right) \left( (\widehat{t_i} \times \widehat{t_j}) \cdot \widehat{R_{ij}} \right) \right] + \left[ \left( 2j_1 - \frac{2j_2}{q} \right) \left( (\widehat{t_i} \times \widehat{R_{ij}}) \cdot (\widehat{t_j} \times \widehat{R_{ij}}) \right) \left( (\widehat{t_i} \times \widehat{t_j}) \cdot \widehat{R_{ij}} \right) \right] \right\} \right\} \left( sin\frac{\theta}{2} + sin^3\frac{\theta}{2} \right) \tag{5}$$

Here, $j_1$ and $j_2$ are first and second order spherical Bessel functions with the argument defined by the scattering wave vector ($q$), $\lambda$ is the wavelength of excitation, $\hat{x}$, $\hat{y}$ and $\hat{z}$ are orthogonal unit vectors in the laboratory frame and $\tau_0$ defines the angular separation between individual point scatterers on the helix. Here, each individual helical strand is defined as a thin-wire, which implies that the polarizibility vectors ($\widehat{t_i}, \widehat{t_j}$) of all point polarizable groups ($i, j$) are tangential to the helix. For helices with tangential polarizibility, the CIDS ratio is independent of the actual polarizibility magnitude, which significantly simplifies the CIDS calculations.[20] Further, we only focus on the CIDS signals outside the absorption band, meaning that dispersive properties of the scatterers are not in the picture. It must be noted that we only focus on the CIDS signals outside the absorption band, meaning that dispersive properties of the scatterers aren't included.

Under the set of assumptions, the independent parameters which control the shape of the CIDS spectrum of an orientationally averaged helix are the helical pitch ($P$), radius ($a$) and the wavelength of incident excitation ($\lambda$). The CIDS spectrum can be conveniently analyzed as a function of the ratio between $P$ and $a$, defined as $\rho$ ($\rho = P/a$) for different values of $\sigma$ ($\sigma = \lambda/P$). Here, $\rho$ is an intrinsic parameter which is dependent on the shape of the helix while $\sigma$ depends on the wavelength of the incident light.

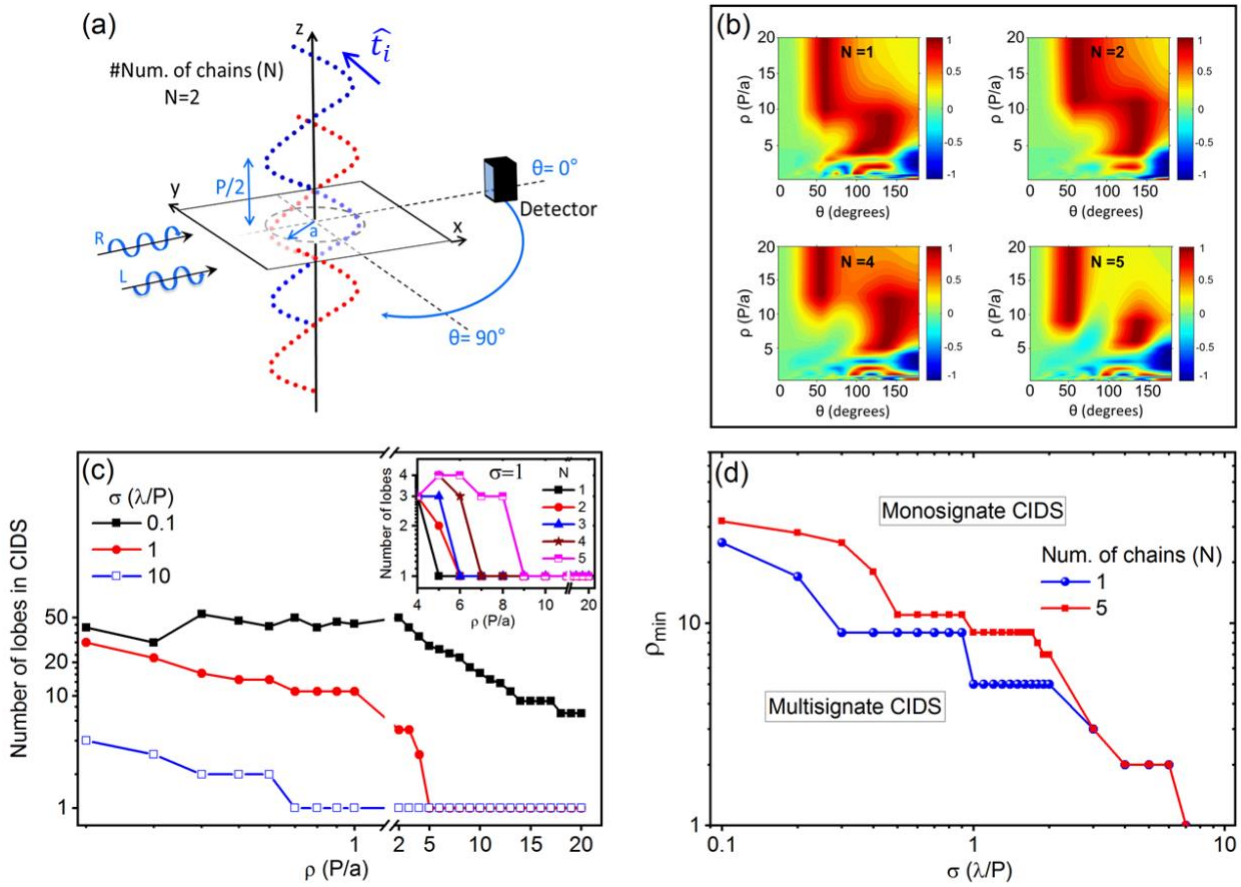


**Figure 1.** (a) Schematic of CIDS model showing a segment of a helical bundle comprising two left-handed helical chains (defined by point polarizable groups) oriented parallel to the z axis in the laboratory frame. The helix pitch ($P$), radius ($a$), the tangential polarizibility ($\hat{t}_i$) and the azimuthal angle ($\theta$) are also depicted. (b) Calculated (normalized) CIDS spectra as a function of $\rho$ for orientationally averaged helical bundles made up of N number of individual chains. (c) The dependence of the number of lobes in the CIDS spectrum on $\rho$ for a single chain at different ratios of $\sigma$ and (inset) helical bundles for $\sigma$ = 1. (d) Minimum value of $\rho$ ($\rho_{min}$) for obtaining a monosignate CIDS spectrum for helical bundles as a function of the ratio $\sigma$. The number of lobes in figure 1c and 1d are calculated by considering the CIDS spectra in the azimuthal angle range 0 to 180°.

To understand the relationship between CIDS response and fibril geometry, we first calculate the CIDS response of an orientationally averaged individual helical chain (N = 1). For given values of $\rho$ and $\sigma$, the sign and magnitude of the CIDS spectrum of a chain are determined by its handedness and total length, respectively. For a chain of a given length and pitch, the increase in the wavelength of excitation (increase in $\sigma$) results in a concomitant decrease in CIDS magnitude. This implies that significant non-zero CIDS response as determined by the instrument sensitivity (typically ~ $10^{-3}$) can only be obtained if the wavelength of incident excitation is not too large in comparison to the pitch of the helical structure (for example, CIDS > $10^{-3}$ if $\sigma < 20$). With reference to nano-materials where the helical pitch is less than few tens of nanometers, measuring non-zero CIDS with visible excitation necessitates improvements in the instrument sensitivity. This can be possible by utilizing state-of the art detection techniques such as incorporation of avalanche photodiodes,[33] electron-multiplying charge coupled devices[34] (EMCCDs) and direct detection of CIDS using detectors made of chiral materials[35].

The shape of the CIDS spectrum of a single helical chain is controlled by the parameters $\rho$ and $\sigma$. Specifically, for a given value of $\sigma$, a threshold value ($\rho_{\min}$) can be defined such that a chain characterized by $\rho$ values larger than $\rho_{\min}$ exhibits a monosignate CIDS spectrum (Figure 1b, c). For example, if $P$ and $\lambda$ are equal ($\sigma = 1$), a monosignate CIDS spectrum will be observed for a helical chain where the pitch is at least 5 times the radius ($\rho_{min} = 5$). Alternatively, chains characterized by very small values of $\rho$ ($\rho < \rho_{min}$) will always exhibit a multisignate CIDS spectrum, marked by multiple positive and negative lobes in the CIDS spectrum. We find that the threshold value $\rho_{min}$ is negatively correlated with $\sigma$, i.e., $\rho_{\min}$ is small if $\sigma$ is high (Figure 1d). For a majority of self-assembled helical fibers of conjugated systems reported in the literature, the helical pitch of a polymer chain is usually of the order of tens of nanometers.[36] Hence, CIDS response at visible wavelengths is expected to be generally monosignate in nature.

In addition to the sensitivity of the shape of the CIDS response on the helix geometry defined by $\rho$, it is also sensitive to bundling of individual helical chains. The most significant effect of bundling of chains is on the value of $\rho_{min}$(Figure 1c, d) where an increase in the number of helical chains (N) comprising a bundle, results in an increase in $\rho_{min}$. This implies that for a helical bundle of a specific geometry (fixed $\rho$) and a given incident wavelength (fixed $\sigma$), an increase in N should increase the number of lobes in the CIDS spectrum. It should be noted that the minimum number of chains necessary to affect the CIDS spectrum of a bundle depends on $\sigma$ such that intertwining of a higher number of individual chains is required if $\sigma$ is large. The sensitivity of the CIDS response to the helix geometry and bundling makes it an efficient probe to reveal the internal structure of fibrillar morphology in self-assembled supramolecular structures.

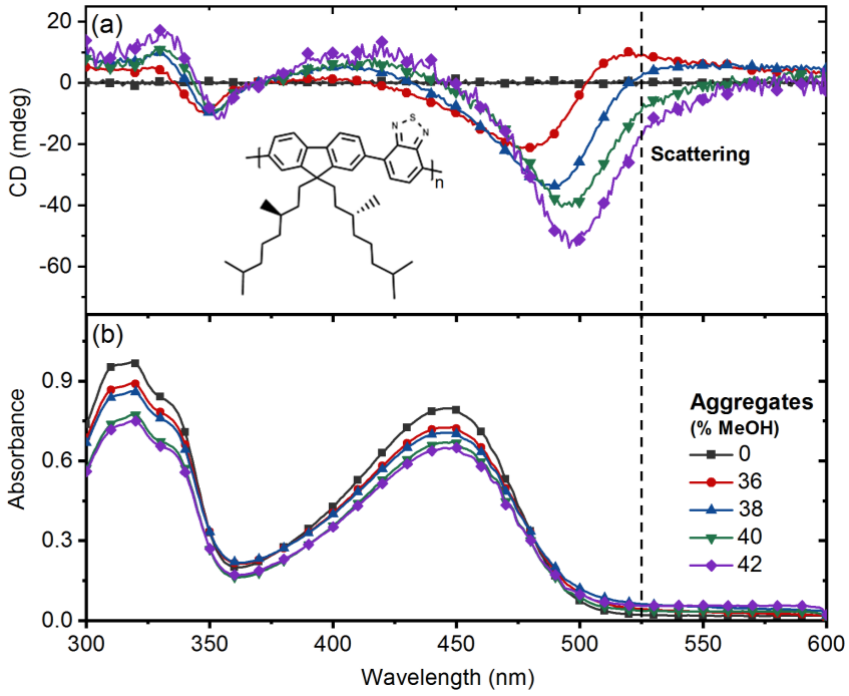


**Figure 2**. (a) CD and (b) absorbance spectra for a 6 µg/ml solution of PFBT in chloroform solution containing different percentages of methanol. Inset figure (a) shows the molecular structure of PFBT.

To demonstrate the utility of our model, we applied it to reproduce CIDS measurements on kinetically self-assembled aggregates of chiral PFBT that form fibrillar structures. Recently, scattering from PFBT fibrils in cholesteric thin films has been proposed to account for an unprecedented high magnitude of circularly polarized electroluminescence observed from PFBT polymer light emitting diodes.[37]

Kinetically controlled self-assembly of PFBT was achieved by dissolving PFBT in chloroform, followed by stepwise addition of the 'bad solvent' methanol to the molecularly dissolved solution. The aggregation of PFBT polymer chains into helical supramolecular structures is confirmed by exciton coupled CD (Figure 2a), consistent with the previous reports.[31, 38] Increase in the magnitude of CD with increasing aggregate size indicates the growth of helical ordering within the aggregates. Interestingly, a non-zero CD is observed well outside the absorption band edge ($\lambda$ > 525 nm) arising due to circularly intensity differential scattering (CIDS). To differentiate the chiroptical response originating from CD and CIDS, we utilized fluorescence detected circular dichroism (FDCD) measurements.

Unlike CD spectroscopy that probes differential transmission of left (L) and right (R) circularly polarized light to obtain complimentary value of $\Delta A$ $(= A_L - A_R)$, FDCD measures the difference in the total intensity of emission upon L and R circularly polarized excitations. As a result, FDCD is insensitive to chiroptical responses originating from scattering and is has been used to decouple intrinsic CD from CIDS.[39-40] For dilute solutions, the measured FDCD signal $(\theta_F)$ is related to $\Delta A$, given the absorbance (A) of the solution is known (equation 2).

$$\theta_F(mdeg) = \frac{32982\Delta A}{(10^A - 1)} \qquad (2)$$

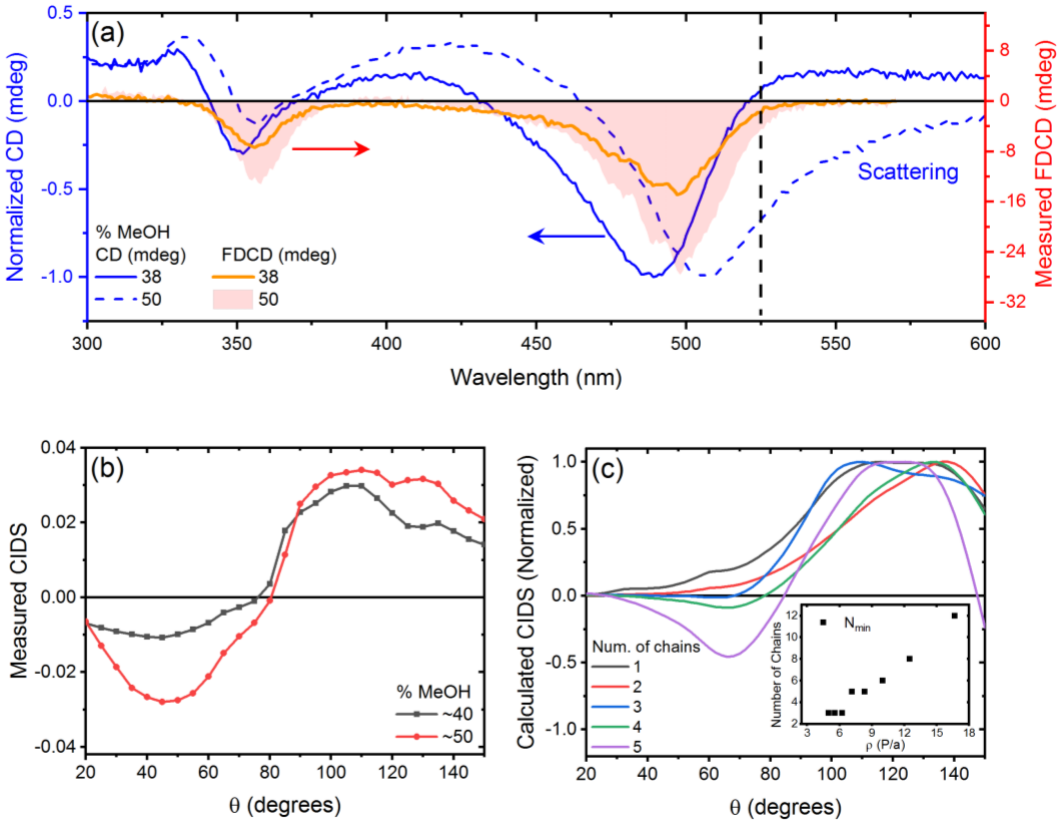


**Figure 3.** (a) Experimental CD (blue lines) and FDCD (orange line and pink shaded area) and (b) experimental CIDS spectra of PFBT aggregates in chloroform and methanol at two different volume percentages (λ=600 nm, bandwidth =20 nm). The lack of FDCD beyond absorbance band edge (525 nm) in (a) confirms that CD spectra at long-wavelengths arise solely due to CIDS. (c) Calculated CIDS of a helical bundle comprised of different number of helical chains for $\rho$ = 5 and $\sigma$ = 1. Inset figure shows a relationship between minimum number of chains in a bundle ($N_{min}$) and $\rho$ required to yield a zero-crossing in the CIDS spectrum.

The shape and sign of the FDCD spectra of kinetically controlled PFBT aggregates obtained at different percentages of methanol in the solvent mixture are very similar and agree well with the characteristic FDCD spectrum of thermodynamically assembled PFBT nano-fibers, reported by us previously.[38] As shown in figure 3a, no appreciable FDCD is observed in the wavelength region outside

the absorption band edge of polymer aggregates ($\lambda$ > 525 nm, region to the right of vertical dashed line) confirming that the CD spectra at long wavelengths can solely be attributed to CIDS.[39] Surprisingly, CD at these wavelengths for larger aggregates formed at higher percentage of methanol is of an opposite sign compared to smaller aggregates. This suggests that aggregate size must significantly influence CIDS. To identify the effect of increasing amount of aggregation on CIDS and understand how these changes relate to the aggregate morphology, we performed CIDS measurements using a custom-made setup (See SI).

As shown in figure 3b, PFBT aggregates in methanol and chloroform solvent mixtures exhibit significant CIDS as a function of azimuthal angle $(\theta)$. With increasing methanol content, CIDS is marked by the growth of a negative spectral lobe between $\theta = 30°$ and $70°$, indicating an increase in scattered intensity of R circularly polarized light. The change in the sign of the CD in PFBT aggregates outside the absorption band edge is consistent with the observed changes in CIDS where R circularly polarized light is scattered more as aggregate size increases, hence resulting in a change in sign of CD.

Using the above model, changes in the shape of the CIDS spectra with increasing aggregation can be reproduced by considering a polymer aggregate as a bundle of a few intertwined polymer chains. It should be noted that the minimum number of single chains in a bundle ($N_{min}$) required to affect the shape of the CIDS spectrum is dependent on the pitch and radius of the helical chains as well as the incident wavelength. Specifically, $N_{min}$ is directly correlated to the parameter $\rho$, i.e., $N_{min}$ is large if the individual strands are thin (small radius). Assuming that the helix pitch is at least 5 times the radius ($\rho \geq 5$) as is usually observed for polymer aggregates[36] and for the limiting case of $\sigma$ = 1, we infer that helical intertwining of at least 5 polymer chains is necessary to explain the observed growth of the bisignate feature observed in the experimental CIDS spectra of PFBT aggregates.

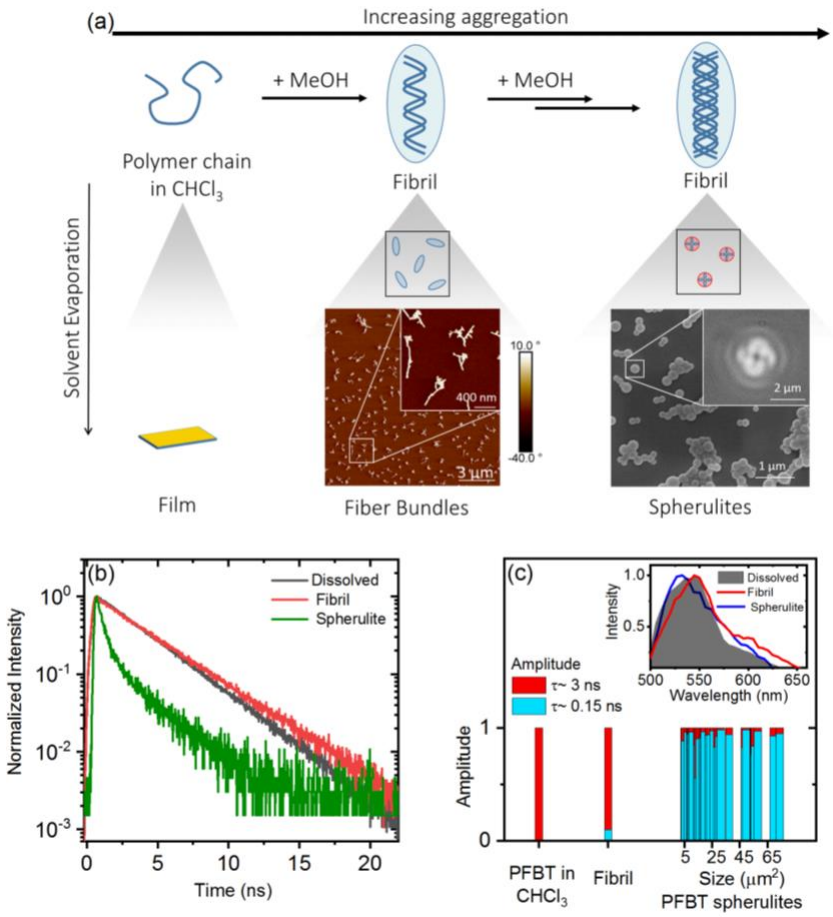


**Figure 4.** (a) Schematic of the evolution of the morphology and the internal structure of PFBT aggregates. Shown also are atomic force microscopy (AFM) phase and scanning electron microscopy (SEM) images of PFBT aggregates drop-casted from a dilute solution containing 30% and concentrated solution containing excess of 50% methanol, respectively. While AFM displays fibrillar aggregates, SEM shows larger aggregates exist as spherulites. Inset in SEM image is zoomed-in polarizing optical micrograph of PFBT spherulites showing Maltese cross pattern. (b) Fluorescence intensity decay curves and (c) histogram of the fluorescence lifetimes for isolated PFBT chains in chloroform, PFBT fibrils and spherulites measured using fluorescence lifetime imaging microscopy. Inset figure compares the emission spectra of isolated PFBT chains, fibrils and spherulites.

Atomic force microscopy (AFM) phase image of PFBT aggregates drop-casted from a dilute PFBT solution containing 30% methanol confirms that polymer aggregates are fibrillar in nature (Figure 4a). This is consistent with our hypothesis that aggregates are indeed bundles of intertwined polymer chains. Based on the insights from Dynamic Light Scattering measurements of fibrils (see SI) and AFM images of drop-casted fibrils, the length of the PFBT fibrils can be estimated to be greater than 100 nm while their respective radii to be less than 30-40 nm's. These bundles exist as fibrils and are also building blocks of larger semi-crystalline structures such as spherulites, formed due to slow evaporation of solvent in drop-cast films of concentrated PFBT solutions containing an excess of 50% methanol. Remarkably, the internal morphology of these spherulites appears to arise from self-sorting of PFBT fibrils. This is confirmed by the characteristic Maltese cross pattern in the polarizing optical micrograph image of the PFBT spherulites, consistent with previous reports.[41-42] Furthermore, emission spectra of individual spherulites are very similar to the emission spectra of PFBT fibrils confirming that fibril are building blocks of these spherulites. The effect of bundling is also reflected in the emission decay dynamics of the fibrils and spherulites. In contrast to the isolated polymer chains in chloroform, PFBT fibrils as well as spherulites exhibit an additional fast decay component. While the contribution from the fast component on the overall emission is small for PFBT fibrils (< 10%), extensive bundling in spherulites impacts the decay dynamics such that the fast component accounts for more than 90% of the overall emission lifetime. The appearance of the fast decay component with increasing aggregation is consistent with previous reports on the emergence of aggregation induced non-radiative decay pathways for PFBT polymer chains.[38]

Based on FDCD, CIDS and microscopy measurements we propose the following schematic of polymer aggregation (Figure 4a). PFBT chains are randomly oriented and molecularly dissolved in chloroform, as confirmed by the lack of any net CD response. Addition of the bad solvent (methanol) results in aggregation of polymer chains into fibrillar geometries. CIDS measurements show that the

fibrils are formed as a result of intertwining of at least 5 polymer chains. At high aggregation levels, enforced by precipitation of the polymer chains in solution and slow evaporation of methanol, the fibrils self-organize into a spherulite shaped geometry.

In conclusion, we advocate the potential of utilizing CIDS, that is usually disregarded as a CD artifact, to develop detailed insights on the internal structure of self-assembled aggregates in solutions. For example, utilizing CIDS on self-assembled PFBT fibrils, we have shown that intertwining of polymer chains is a primary process in the formation of PFBT fibrils. We anticipate that similar conclusions can be drawn on for a wide range of other π -conjugated systems, which involve self-assembly of isolated molecules into fiber-like supramolecular structures.

**Supporting Information**

Details on the experimental procedures are provided in the ESI. The ESI also includes details about the CIDS setup, the theoretical formalism of CIDS and supporting figures for the various techniques discussed in the main text.

**Conflicts of interest**

There are no conflicts to declare.

**Acknowledgements**

The authors thank Dr. Robert Abbel for the generous gift of the polymer material.

**References**

1. Günes, S.; Neugebauer, H.; Sariciftci, N. S., Conjugated Polymer-Based Organic Solar Cells. *Chem. Rev.* **2007**, *107*, 1324-1338.

2. Jackson, N. E.; Kohlstedt, K. L.; Savoie, B. M.; Olvera de la Cruz, M.; Schatz, G. C.; Chen, L. X.; Ratner, M. A., Conformational Order in Aggregates of Conjugated Polymers. *J. Am. Chem. Soc.* **2015**, *137*, 6254-6262.

3. Hoeben, F. J. M.; Jonkheijm, P.; Meijer, E. W.; Schenning, A. P. H. J., About Supramolecular Assemblies of Π-Conjugated Systems. *Chem. Rev.* **2005**, *105*, 1491-1546.

4. Liu, T.; Huo, L.; Chandrabose, S.; Chen, K.; Han, G.; Qi, F.; Meng, X.; Xie, D.; Ma, W.; Yi, Y., et al., Optimized Fibril Network Morphology by Precise Side-Chain Engineering to Achieve High-Performance Bulk-Heterojunction Organic Solar Cells. *Adv. Mater.* **2018**, *30*, 1707353.

5. Tian, L.; Szilluweit, R.; Marty, R.; Bertschi, L.; Zerson, M.; Spitzner, E.-C.; Magerle, R.; Frauenrath, H., Development of a Robust Supramolecular Method to Prepare Well-Defined Nanofibrils from Conjugated Molecules. *Chem. Sci.* **2012**, *3*, 1512-1521.

6. Liu, F.; Wang, C.; Baral, J. K.; Zhang, L.; Watkins, J. J.; Briseno, A. L.; Russell, T. P., Relating Chemical Structure to Device Performance Via Morphology Control in Diketopyrrolopyrrole-Based Low Band Gap Polymers. *J. Am. Chem. Soc.* **2013**, *135*, 19248-19259.

7. Knaapila, M.; Stepanyan, R.; Torkkeli, M.; Lyons, B. P.; Ikonen, T. P.; Almásy, L.; Foreman, J. P.; Serimaa, R.; Güntner, R.; Scherf, U., et al., Influence of Molecular Weight on the Phase Behavior and Structure Formation of Branched Side-Chain Hairy-Rod Polyfluorene in Bulk Phase. *Phys. Rev. E* **2005**, *71*, 13.

8. Traiphol, R.; Charoenthai, N.; Srikhirin, T.; Perahia, D., Self-Assembling into Interconnected Nanoribbons in Thin Films of Hairy Rod Poly(9,9-Di(2-Ethylhexyl)Fluorene): Effects of Concentration, Substrate and Solvent. *Synth. Met.* **2010**, *160*, 1318-1324.

9. Xu, L.; Zhang, J.; Peng, J.; Qiu, F., Formation of Nanofibers in Poly(9,9-Dioctylfluorene) Toluene Solutions During Aging. *J. Polym. Sci., Part B: Polym. Phys.* **2015**, *53*, 633-639.

10. Fytas, G.; Nothofer, H. G.; Scherf, U.; Vlassopoulos, D.; Meier, G., Structure and Dynamics of Nondilute Polyfluorene Solutions. *Macromolecules* **2002**, *35*, 481-488.

11. Chabinyc, M. L., X-Ray Scattering from Films of Semiconducting Polymers. *Polym. Rev.* **2008**, *48*, 463-492.

12. Knaapila, M.; Bright, D. W.; Stepanyan, R.; Torkkeli, M.; Almásy, L.; Schweins, R.; Vainio, U.; Preis, E.; Galbrecht, F.; Scherf, U., et al., Network Structure of Polyfluorene Sheets as a Function of Alkyl Side Chain Length. *Phys. Rev. E* **2011**, *83*, 11.

13. Brinkmann, M.; Charoenthai, N.; Traiphol, R.; Piyakulawat, P.; Wlosnewski, J.; Asawapirom, U., Structure and Morphology in Highly Oriented Films of Poly(9,9-Bis(N-Octyl)Fluorene-2,7-Diyl) and Poly(9,9-Bis(2-Ethylhexyl)Fluorene-2,7-Diyl) Grown on Friction Transferred Poly(Tetrafluoroethylene). *Macromolecules* **2009**, *42*, 8298-8306.

14. Knaapila, M.; Torkkeli, M.; Monkman, A. P., Evidence for 21-Helicity of Poly[9,9-Bis(2-Ethylhexyl)Fluorene-2,7-Diyl]. *Macromolecules* **2007**, *40*, 3610-3614.

15. Knaapila, M.; Lyons, B. P.; Kisko, K.; Foreman, J. P.; Vainio, U.; Mihaylova, M.; Seeck, O. H.; Pålsson, L.-O.; Serimaa, R.; Torkkeli, M., et al., X-Ray Diffraction Studies of Multiple Orientation in Poly(9,9-Bis(2-Ethylhexyl)Fluorene-2,7-Diyl) Thin Films. *J. Phys. Chem. B* **2003**, *107*, 12425-12430.

16. Lakhwani, G.; Gielen, J.; Kemerink, M.; Christianen, P. C. M.; Janssen, R. A. J.; Meskers, S. C. J., Intensive Chiroptical Properties of Chiral Polyfluorenes Associated with Fibril Formation. *J. Phys. Chem. B* **2009**, *113*, 14047-14051.

17. Goto, H.; Okamoto, Y.; Yashima, E., Solvent-Induced Chiroptical Changes in Supramolecular Assemblies of an Optically Active, Regioregular Polythiophene. *Macromolecules* **2002**, *35*, 4590-4601.

18. Amrutha, S. R.; Jayakannan, M., Probing the Π-Stacking Induced Molecular Aggregation in Π-Conjugated Polymers, Oligomers, and Their Blends of P-Phenylenevinylenes. *J. Phys. Chem. B* **2008**, *112*, 1119-1129.

19. Bustamante, C.; Jr., I. T.; Maestre, M. F., Circular Intensity Differential Scattering of Light. Iv. Randomly Oriented Species. *J. Chem. Phys.* **1982**, *76*, 3440-3446.

20. Bustamante, C.; Maestre, M. F.; Jr., I. T., Circular Intensity Differential Scattering of Light by Helical Structures. I. Theory. *J. Chem. Phys.* **1980**, *73*, 4273-4281.

21. Bustamante, C. J.; Wells, K. S.; Keller, D.; Samori, B.; Maestre, M. F.; Tinoco, I., The Circular Intensity Differential Scattering (Cids) of Cholesteric and Blue Mesophases. *Mol. Cryst. Liq. Cryst.* **1984**, *111*, 79-102.

22. Belmont, A. S.; Zietz, S.; Nicolini, C., Differential Scattering of Circularly Polarized Light by Chromatin Modeled as a Helical Array of Dielectric Ellipsoids within the Born Approximation. *Biopolymers* **1985**, *24*, 1301-1321.

23. Diaspro, A.; Nicolini, C. A., Circular Intensity Differential Scattering and Chromatin-DNA Structure. *Cell Biophys.* **1987**, *10*, 45-60.

24. Maestre, M. F.; Bustamante, C.; Hayes, T. L.; Subirana, J. A.; Tinoco, I., Differential Scattering of Circularly Polarized Light by the Helical Sperm Head from the Octopus Eledone Cirrhosa. *Nature* **1982**, *298*, 773-774.

25. Shapiro, D. B.; Hull, P. G.; Shi, Y.; Quinby-Hunt, M. S.; Maestre, M. F.; Hearst, J. E.; Hunt, A. J., Toward a Working Theory of Polarized Light Scattering from Helices. *J. Chem. Phys.* **1994**, *100*, 146-157.

26. Yoo, S.; Park, Q. H., Enhancement of Chiroptical Signals by Circular Differential Mie Scattering of Nanoparticles. *Sci. Rep.* **2015**, *5*, 14463.

27. Spada, G. P.; Gottarelli, G.; Samori, B.; Bustamante, C. J.; Wells, K. S., A Study of Some Lyotropic Cholesteric Mesophases by Circular and Linear Dichroism and by Circular Intensity Differential Scattering. *Liq. Cryst.* **1988**, *3*, 101-113.

28. Lakhwani, G.; Meskers, S. C. J.; Janssen, R. A. J., Circular Differential Scattering of Light in Films of Chiral Polyfluorene. *J. Phys. Chem. B* **2007**, *111*, 5124-5131.

29. Bustamante, C.; Maestre, M. F.; Keller, D., Expressions for the Interpretation of Circular Intensity Differential Scattering of Chiral Aggregates. *Biopolymers* **1985**, *24*, 1595-1612.

30. Craig, M. R.; Jonkheijm, P.; Meskers, S. C. J.; Schenning, A. P. H. J.; Meijer, E. W., The Chiroptical Properties of a Thermally Annealed Film of Chiral Substituted Polyfluorene Depend on Film Thickness. *Adv. Mater.* **2003**, *15*, 1435-1438.

31. Kulkarni, C.; Di Nuzzo, D.; Meijer, E. W.; Meskers, S. C. J., Pitch and Handedness of the Cholesteric Order in Films of a Chiral Alternating Fluorene Copolymer. *J. Phys. Chem. B* **2017**, *121*, 11520-11527.

32. Shapiro, D. B.; Maestre, M. F.; McClain, W. M.; Hull, P. G.; Shi, Y.; Quinby-Hunt, M. S.; Hearst, J. E.; Hunt, A. J., Determination of the Average Orientation of DNA in the Octopus Sperm Eledone Cirrhossa through Polarized Light Scattering. *Appl. Opt.* **1994**, *33*, 5733-5744.

33. Le Gratiet, A.; Pesce, L.; Oneto, M.; Marongiu, R.; Zanini, G.; Bianchini, P.; Diaspro, A., Circular Intensity Differential Scattering (Cids) Scanning Microscopy to Image Chromatin-DNA Nuclear Organization. *OSA Continuum* **2018**, *1*, 1068-1078.

34. Hassey, R.; McCarthy, K. D.; Swain, E.; Basak, D.; Venkataraman, D.; Barnes, M. D., Single-Molecule Chiroptical Spectroscopy: Fluorescence Excitation of Individual Helicene Molecules in Polymer-Supported Thin-Films. *Chirality* **2008**, *20*, 1039-1046.

35. Chen, C.; Gao, L.; Gao, W.; Ge, C.; Du, X.; Li, Z.; Yang, Y.; Niu, G.; Tang, J., Circularly Polarized Light Detection Using Chiral Hybrid Perovskite. *Nat. Commun.* **2019**, *10*, 1927.

36. Yashima, E.; Ousaka, N.; Taura, D.; Shimomura, K.; Ikai, T.; Maeda, K., Supramolecular Helical Systems: Helical Assemblies of Small Molecules, Foldamers, and Polymers with Chiral Amplification and Their Functions. *Chem. Rev.* **2016**, *116*, 13752-13990.

37. Di Nuzzo, D.; Kulkarni, C.; Zhao, B.; Smolinsky, E.; Tassinari, F.; Meskers, S. C. J.; Naaman, R.; Meijer, E. W.; Friend, R. H., High Circular Polarization of Electroluminescence Achieved Via Self-Assembly of a

Light-Emitting Chiral Conjugated Polymer into Multidomain Cholesteric Films. *ACS Nano* **2017**, *11*, 12713-12722.

38. Sharma, A.; Athanasopoulos, S.; Tapping, P. C.; Sabatini, R. P.; McRae, O. F.; Müllner, M.; Kee, T. W.; Lakhwani, G., Emission Decay Pathways Sensitive to Circular Polarization of Excitation. *J. Phys. Chem. C* **2018**, *122*, 23910-23916.

39. Tinoco, I.; Maestre, M. F.; Bustamante, C., Circular Dichroism in Samples Which Scatter Light. *Trends Biochem. Sci* **1983**, *8*, 41-44.

40. Tinoco, I.; Turner, D. H., Fluorescence Detected Circular Dichroism. Theory. *J. Am. Chem. Soc.* **1976**, *98*, 6453-6456.

41. Adachi, T.; Tong, L.; Kuwabara, J.; Kanbara, T.; Saeki, A.; Seki, S.; Yamamoto, Y., Spherical Assemblies from Π-Conjugated Alternating Copolymers: Toward Optoelectronic Colloidal Crystals. *J. Am. Chem. Soc.* **2013**, *135*, 870-876.

42. Watanabe, K.; Iida, H.; Akagi, K., Circularly Polarized Blue Luminescent Spherulites Consisting of Hierarchically Assembled Ionic Conjugated Polymers with a Helically Π-Stacked Structure. *Adv. Mater.* **2012**, *24*, 6451-6456.